ELSEVIER

Organic Electronics 2 (2001) 37–43

Organic Electronics

www.elsevier.nl/locate/orgel

Efficient electrophosphorescence using a doped ambipolar conductive molecular organic thin film

Chihaya Adachi [b], Raymond Kwong [a], Stephen R. Forrest [b,*]

[a] *Universal Display Corporation, 375 Phillips Boulevard, Ewing, NJ 08618, USA*

[b] *Department of Electrical Engineering, Center for Photonics and Optoelectronic Materials (POEM), Princeton University, Princeton, NJ 08544, USA*

Received 22 November 2000; accepted 2 February 2001

Abstract

We demonstrate a high efficiency organic electrophosphorescent device comprised of a 4,4′,4″-tris(3-methylphenylphenylamino)triphenylamine (*m*-MTDATA) hole transport layer and a 4,4′-*N*,*N*′-dicarbazole-biphenyl (CBP) host doped with the metallorganic phosphor, *fac*-tris(2-phenylpyridine)iridium ($Ir(ppy)_3$) as the green light-emitting layer. The device exhibits peak external quantum and power efficiencies of $(12.0 \pm 0.6)\%$ and (45 ± 2) lm/W, respectively, corresponding to ~60% internal quantum efficiency. A luminance of 1850 cd/m^2 is observed at a current density of 10 mA/cm^2. The device operating properties are controlled by electron injection into, and transport by the CBP layer along with hole injection from *m*-MTDATA directly into the $Ir(ppy)_3$ highest occupied molecular level, leading to direct carrier recombination and exciton formation on the phosphor dopant. Ambipolar conduction properties of the $Ir(ppy)_3$:CBP layer are established by analysis of triplet–triplet annihilation, exciton formation and the luminance–current–voltage characteristics. © 2001 Published by Elsevier Science B.V.

PACS: 72.80.L; 78.60.F; 85.60.J; 33.50.D

Keywords: Electrophosphorescence; Ambipolar conduction; 4,4′-*N*,*N*′-dicarbazole-biphenyl; Triplet–triplet annihilation

High efficiency organic light emitting devices (OLEDs) using the phosphorescent dopant, *fac*-tris(2-phenylpyridine)iridium ($Ir(ppy)_3$), have been demonstrated using several different conducting host materials [1–7]. Since the triplet level of the metal–ligand charge transfer state [8] of the green-emitting $Ir(ppy)_3$ is between 2.5 and 3.0 eV, deep blue fluorophores with a peak wavelength of $\lambda_{peak} \sim 400$ nm, such as 4,4′-*N*,*N*′-dicarbazole-biphenyl (CBP) [2–4,9], are likely candidates as triplet energy transfer and exciton confining media. Using 6% to 10% $Ir(ppy)_3$ in CBP leads to efficient $Ir(ppy)_3$ phosphorescence [3,4]. In addition to the energetic resonance between the dopant and the host, the control of charge carrier injection and transport in the host layers is necessary for achieving efficient formation of radiative excitons [2,3,5]. Indeed, high electrophosphorescence efficiency has been achieved using $Ir(ppy)_3$ doped into CBP along with a 2,9-dimethyl-4,7-diphenyl-phenanthroline (BCP) electron transport and exciton blocking layer [3]. In that device, the doped CBP layer was found to readily transport holes.

* Corresponding author. Tel.: +1-609-258-3500; fax: +1-609-258-0119.

E-mail address: forrest@ee.princeton.edu (S.R. Forrest).

1566-1199/01/$ - see front matter © 2001 Published by Elsevier Science B.V.
PII: S1566-1199(01)00010-6

Here, we demonstrate that CBP can also serve as an electron transporting host in a considerably simplified bilayer structure consisting of an indium tin oxide (ITO) anode, a 4,4′,4″-tris(3-methylphenylphenylamino)triphenylamine (*m*-MTDATA) [10] hole injection layer (HIL), an ambipolar conductive $Ir(ppy)_3$:CBP emissive layer, and a MgAg/Ag cathode. This simplified OLED exhibits an external quantum efficiency (η_{ext}) and power efficiency (η_p) comparable to the best results obtained for more complex heterostructure electrophosphorescent OLEDs [2,3,5]. To investigate the ambipolar transport characteristics of the CBP layers, we determine the locations of the exciton formation zones in two archetype device structures.

Devices studied were fabricated as follows: the organic layers were deposited by high-vacuum (1×10^{-6} Torr) thermal evaporation onto a pre-cleaned ITO coated glass substrate with an ITO sheet resistance of ~20 Ω/□. Prior to film deposition, the substrate was solvent degreased and cleaned in a UV-ozone chamber before it was loaded into the deposition system. For device I, a 50 nm-thick layer of *m*-MTDATA was first deposited, followed by a 60 nm-thick $Ir(ppy)_3$:CBP light emitting and transport layer. Previously [11], *m*-MTDATA has been identified as effective in promoting injection of holes from ITO into hole transport layers (HTL) consisting of, for example 4,4′-bis[*N*-(naphthyl)-*N*-phenyl-amino]biphenyl (α-NPD) or *N*,*N*′-bis(3-methylphenyl)–*N*,*N*′-diphenyl-[1,1'-biphenyl]4,4′-diamine (TPD), possibly due to reduction of the HTL highest occupied molecular orbital (HOMO)/ITO offset energy, or to wetting of the ITO surface. We fixed the $Ir(ppy)_3$ concentration at 7%, since this resulted in the highest η_{ext}. A shadow mask with 1 mm diameter openings was used to define the cathodes consisting of a 100 nm-thick layer of 25:1 Mg:Ag with a 20 nm-thick Ag cap. A conventional heterostructure device (device II), consisting of ITO/α-NPD (50 nm)/7%-$Ir(ppy)_3$:CBP (20 nm)/BCP (10 nm)/tris(8-hydroxyquinoline)aluminum (Alq_3) (40 nm)/Mg–Ag (100 nm)/Ag (20 nm) [3], was fabricated for comparison. To locate the exciton formation zone, we employed a local doping technique [12–17] where a thin 7%-$Ir(ppy)_3$:CBP light emissive slab was grown into the CBP host layer at varying distances between the cathode and anode contacts.

The energy level diagrams of devices I and II are shown in Fig. 1 [18,19]. The positions of the $Ir(ppy)_3$ HOMO and lowest unoccupied molecular orbital (LUMO) levels relative to those of CBP were estimated using a combination of ultraviolet photoelectron and optical absorption spectroscopy. Phosphorescence emission spectra of CBP and *m*-MTDATA were obtained at 70 K using a streak camera (Hamamatsu C4334) in the photon counting mode. A nitrogen gas laser with a wavelength of $\lambda = 337$ nm (Laser Photonics, pulse width ~500 ps) was used as excitation source.

Fig. 2 shows the dependencies of η_{ext} and η_p on current (J) for the devices studied. In device I, a maximum $\eta_{ext} = (12.0 \pm 0.6)\%$ and $\eta_p = (45 \pm 2)$ lm/W were obtained at low currents ($J < 0.1$ mA/cm^2), which is significantly higher than $\eta_{ext} = (8.0 \pm 0.6)\%$ for device II. A luminance of 1850 cd/m^2 is observed at a current density of 10 mA/cm^2. Thus, the simplified device architecture exhibits efficient radiative decay of $Ir(ppy)_3$ triplet excitons due to balanced hole and electron injection into the $Ir(ppy)_3$:CBP light emitting layer.

The gradual roll-off in η_{ext} with increasing current has previously been ascribed to triplet–triplet (T–T) annihilation [20,21], in which case

$$\eta_{ext} = \frac{\eta_0 J_0}{4J}\left(\sqrt{1 + 8\frac{J}{J_0}} - 1\right), \tag{1}$$

where

$$J_0 = \frac{4qd}{\kappa_{TT}\tau^2}. \tag{2}$$

Here, q is the electron charge, d is the thickness of the exciton formation zone, τ is the phosphorescent lifetime, and κ_{TT} is the T–T annihilation quenching parameter. Now, $\eta_{ext} = \eta_0$ at $J = 0$, and when $J = J_0$, then $\eta_{ext} = \frac{1}{2}\eta_0$. From the figure (solid lines), a best fit of the model to the data for devices I and II gives $J_{0(I)} = 5.5$ and $J_{0(II)} = 200$ mA/cm^2, respectively. The ratio of $J_{0(II)}/J_{0(I)} \cong 36$ implies that the width of the exciton formation zone (d) in device I is significantly narrower than that of device II (thus leading to a high local concentration of triplets and hence increased T–T annihilation),

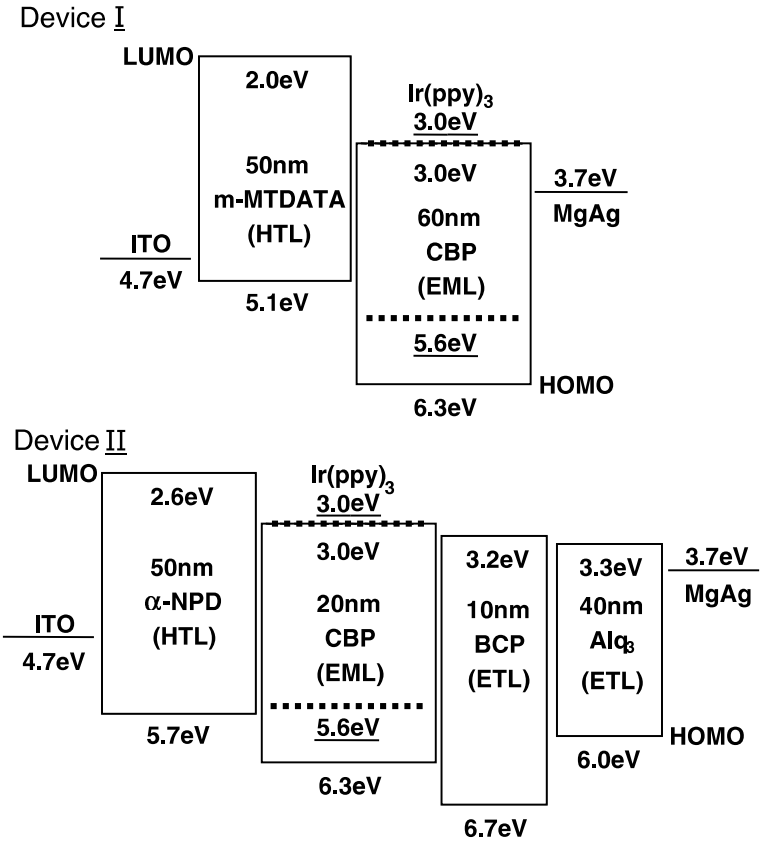

Fig. 1. Proposed energy level diagrams of two device structures showing the relative positions of the HOMO and LUMO levels of the organic layers used in this study. The $Ir(ppy)_3$ LUMO (3.0 eV) is aligned with the CBP LUMO, assuming that the singlet energy of the metal–ligand charge transfer state is at 2.6 eV as obtained from the $Ir(ppy)_3$ and CBP absorption spectra.

assuming that κ_{TT} is a material property independent of excitation density and device structure [21].

To understand the origin of the high η_{ext} in device I, the location of the exciton formation zone was determined by employing a 5 nm-thick 7%-$Ir(ppy)_3$:CBP slab located at various positions within the 20 nm-thick CBP transport layer. The doped layer was systematically moved from the *m*-MTDATA/$Ir(ppy)_3$:CBP (device I) or α-NPD/$Ir(ppy)_3$:CBP (device II) interface to the cathode side. Figs. 3 and 4 show the variations of η_{ext} and the electroluminescence spectra as functions of the distance (d_s) of the doped layer from these interfaces.

For device I (filled circles in Fig. 3), $\eta_{ext} = (7.0 \pm 0.5)\%$ is obtained with $d_s = 0$ nm, decreasing rapidly with increasing d_s. Although only $Ir(ppy)_3$ triplet emission ($\lambda_{max} \sim 515$ nm) was observed for $d_s = 0$ nm (Fig. 4(a)), the contribution from $Ir(ppy)_3$ gradually decreases, accompanied by an increase of blue emission (with peaks at $\lambda_{max} = 430$ and $\lambda_s = 455$ nm) with increasing d_s. The blue emission is due to *m*-MTDATA fluorescence, leading to two conclusions. The $Ir(ppy)_3$:CBP layer predominantly (although not exclusively) transports *electrons* since carrier recombination and exciton formation occur within 10 nm of the *m*-MTDATA/$Ir(ppy)_3$:CBP interface. This is consistent with the observation that the $Ir(ppy)_3$ LUMO energy is approximately equal to that of CBP (3.0 eV) (Fig. 1). Furthermore, $Ir(ppy)_3$ excitons are formed through direct hole injection from *m*-MTDATA into the $Ir(ppy)_3$ HOMO levels. This is apparent since the exciton formation zone moves

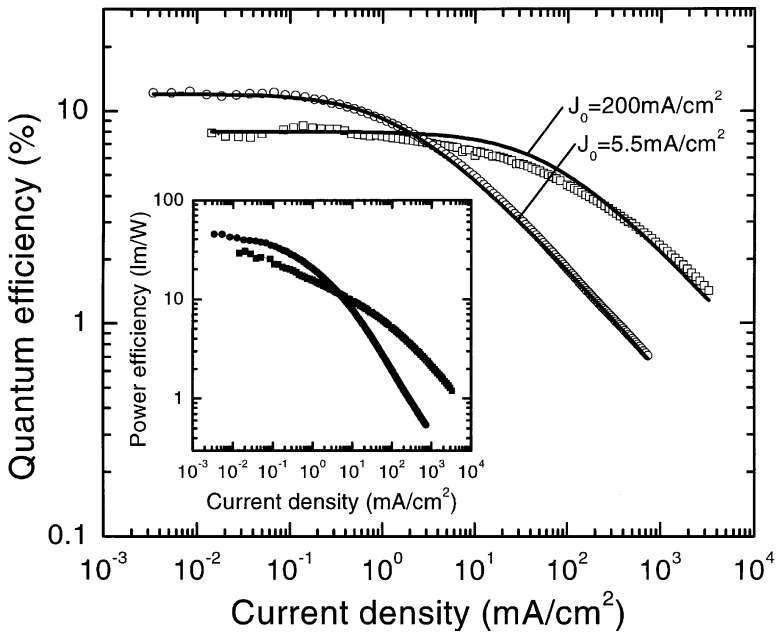

Fig. 2. External quantum efficiency (η_{ext}) versus current density for devices I (○) and II (□). A maximum $\eta_{ext} = 12.0 \pm 0.6\%$ was obtained in device I. The solid line is a fit of the triplet–triplet annihilation model of Eqs. (1) and (2) to the data using $J_0 = 5.5$ mA/cm^2 for device I and 200 mA/cm^2 for device II. Also shown is the power efficiency (η_p) versus current density for devices I (●) and II (■). A maximum $\eta_{ext} = 45 \pm 3$ lm/W was obtained for device I.

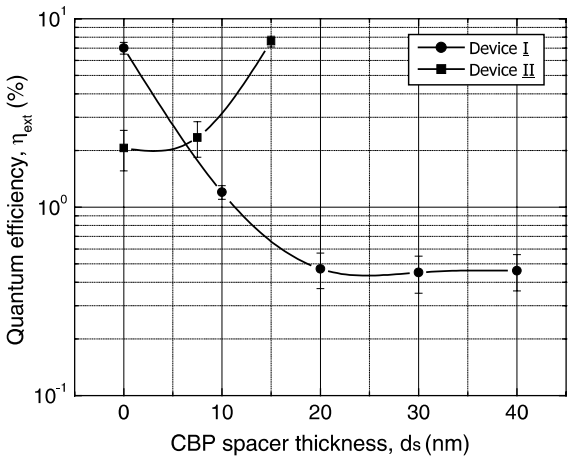

Fig. 3. External quantum efficiency versus the thickness of the CBP spacer layer (η_{ext}–d_s) measured at $J = 0.1$ mA/cm^2 in devices I (●) and II (■). The thicknesses of the doped slab are 20 nm for device I and 5 nm for device II.

with d_s. When the Ir(ppy)$_3$:CBP doped slab is positioned away from the *m*-MTDATA/CBP interface (d_s = 10–40 nm), the spectra are composed of both *m*-MTDATA and Ir(ppy)$_3$ emission. Therefore, holes partly accumulate in the *m*-MTDATA layer in close proximity to the *m*-MTDATA/CBP interface, and recombine with electrons injected from CBP into *m*-MTDATA, leading to *m*-MTDATA exciton formation along with Ir(ppy)$_3$ exciton formation in the Ir(ppy)$_3$-doped CBP slab. Hole accumulation at the *m*-MTDATA/CBP interface results from the large energy barrier (1.2 eV) between the HOMO levels of *m*-MTDATA and CBP. At $d_s = 0$ nm, on the other hand, since we observe no *m*-MTDATA emission, most holes are directly injected from the *m*-MTDATA HOMO (5.1 eV) into the Ir(ppy)$_3$ HOMO (5.6 eV) levels, which recombine with electrons transported by CBP, leading to direct Ir(ppy)$_3$ exciton formation.

The *m*-MTDATA/CBP interface also plays an important role in Ir(ppy)$_3$ triplet exciton confinement. The phosphorescence onset wavelengths of CBP and *m*-MTDATA are at 475 and 490 nm, which are comparable with the Ir(ppy)$_3$ phosphorescent emission peak (Fig. 4(b)). Here, the relaxed

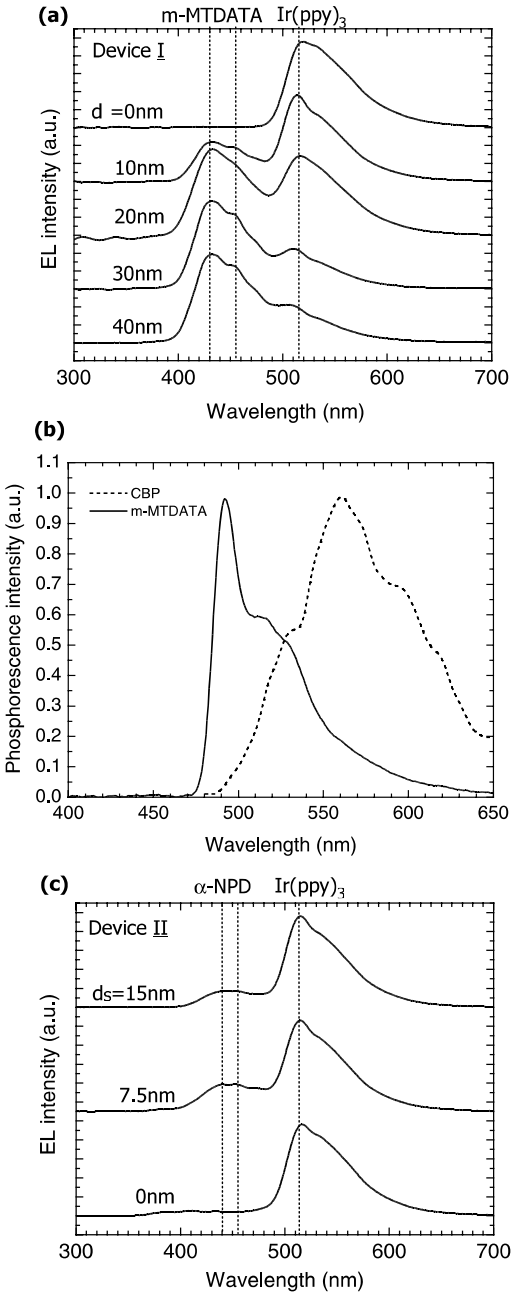

Fig. 4. (a) Electroluminescent spectra of device I as a function of CBP spacer layer thickness, d_s. The peak emission wavelengths of m-MTDATA ($\lambda_{max} = 430$ and 455 nm) and $Ir(ppy)_3$ ($\lambda_{max} = 515$ nm) are indicated. (b) Phosphorescence spectra of CBP (—) and m-MTDATA (- - -) films at 70 K. (c) As in (a) for device II. The peak wavelength of α-NPD ($\lambda_{max} = 440$ and 455 nm) and $Ir(ppy)_3$ ($\lambda_{max} = 515$ nm) are indicated.

$Ir(ppy)_3$ triplet state is at a slightly lower energy compared with the unrelaxed triplet states of CBP and *m*-MTDATA, leading to efficient triplet exciton confinement and radiative decay at the interface. For example, when α-NPD and TPD are employed as HTLs, we find $\eta_{ext} < 6\%$ with an appreciable contribution to the luminescence due to HTL emission. Since the α-NPD LUMO (2.6 eV) is lower than that of *m*-MTDATA, electron injection from $Ir(ppy)_3$:CBP into the HTL occurs, leading to a reduction in η_{ext}.

We note that while the MgAg cathode injects electrons into the doped CBP layer which transports electrons, the existence of $Ir(ppy)_3$ luminescence even for $d_s > 0$ nm suggests that a neat CBP layer also serves as a hole transporting medium following injection from *m*-MTDATA.

For device II, a maximum $\eta_{ext} = (8.0 \pm 0.5)\%$ was observed when a 5 nm-thick $Ir(ppy)_3$:CBP doped layer was placed close to the BCP layer (filled squares in Fig. 3), suggesting that, in this case, $Ir(ppy)_3$:CBP preferentially transports *holes*, and exciton formation mainly occurs near the $Ir(ppy)_3$:CBP/BCP interface. At both $d_s = 7.5$ and 15 nm, the electroluminescence spectra are comprised of two components, $Ir(ppy)_3$ emission at $\lambda_{max} = 515$ nm and α-NPD emission at $\lambda_{max} = 440$ and 455 nm (Fig. 4(c)). The presence of α-NPD emission again suggests hole accumulation at the α-NPD/CBP interface when a neat CBP layer exists between these layers, leading to carrier recombination partly within the HTL.

The *J–V* characteristics in Fig. 5 show that both devices I and II exhibit an abrupt current increase immediately above the turn on voltage, V_T (≅2.5 V). Device I has a slightly lower V_T than does device II due to the reduced voltage drop across the simplified structure. As in the case of single layer polymer devices [22,23], we find that the onset of light emission also occurs at approximately V_T which corresponds to the minimum potential required to form an exciton on an $Ir(ppy)_3$ molecule.

In summary, we demonstrated that an $Ir(ppy)_3$:CBP layer has ambipolar carrier transport characteristics in two device structures. In device I, electrons are injected from a Mg–Ag cathode into CBP, and they subsequently traverse

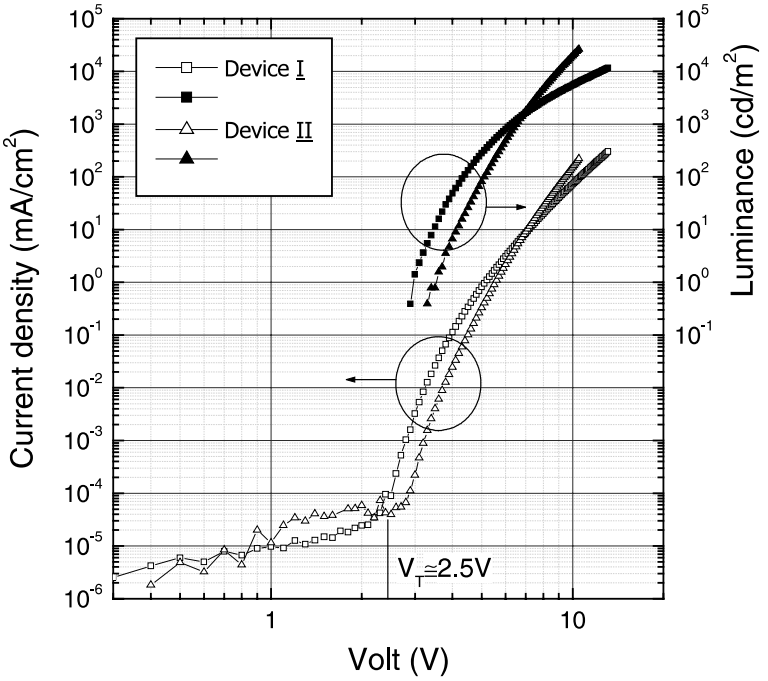

Fig. 5. Luminance–current density–voltage characteristics of devices I (□) and II (△). Note that V_T in device I corresponds to the potential energy of the Ir(ppy)$_3$ metal–ligand charge-transfer state energy.

the layer where they recombine with holes directly injected from *m*-MTDATA into Ir(ppy)$_3$ HOMO levels. In the conventional heterostructure device II, the carrier recombination zone is located near the cathode, suggesting that the Ir(ppy)$_3$:CBP layer also transports holes. Hence, depending on the combination of the carrier injection layers adjacent to the emitting layer, Ir(ppy)$_3$:CBP, can transport either holes or electrons. Using this ambipolar conduction property, an efficient and simple electrophosphorescent OLED was demonstrated.

Acknowledgements

The authors acknowledge C. Shen and Prof. A. Kahn for ultraviolet photoelectron spectroscopy measurements of the Ir(ppy)$_3$ HOMO energy. We also thank M.A. Baldo and Prof. M.E. Thompson for their insightful discussions. This work was funded by Universal Display Corporation, Defense Advanced Research Projects Agency, and Air Force Office of Scientific Research.

References

[1] M.A. Baldo, D.F. O'Brien, Y. You, A. Shoustikov, S. Sibley, M.E. Thompson, S.R. Forrest, Nature 395 (1998) 151.
[2] D.F. O'Brien, M.A. Baldo, M.E. Thompson, S.R. Forrest, Appl. Phys. Lett. 74 (1999) 442.
[3] M.A. Baldo, S. Lamansky, P.E. Burrows, M.E. Thompson, S.R. Forrest, Appl. Phys. Lett. 75 (1999) 4.
[4] T. Tsutsui, M.J. Yang, M. Yahiro, K. Nakamura, T. Watanabe, T. Tsuji, Y. Fukuda, T. Wakimoto, S. Miyaguchi, Jpn. J. Appl. Phys. 38 (Part 2) (1999) L1502.
[5] C. Adachi, M.A. Baldo, S.R. Forrest, Appl. Phys. Lett. 77 (2000) 904.
[6] M.J. Yang, T. Tsutsui, Jpn. J. Appl. Phys. 39 (Part 2) (2000) L828.
[7] C.-L. Lee, K.B. Lee, J.-J. Kim, Appl. Phys. Lett. 77 (2000) 2280.
[8] K.A. King, P.J. Spellane, R.J. Watts, J. Am. Chem. Soc. 107 (1985) 1431.
[9] H. Kanai, S. Ichinosawa, Y. Sato, Synth. Met. 91 (1997) 195.
[10] A. Higuchi, H. Inada, Y. Shirota, Adv. Mater. 3 (1991) 549.
[11] Y. Shirota, Y. Kuwabata, H. Inada, T. Wakimoto, H. Nakada, Y. Yonemoto, S. Kawami, K. Imai, Appl. Phys. Lett. 65 (1994) 807.

[12] C.W. Tang, S.A. VanSlyke, C.H. Chen, J. Appl. Phys. 65 (1989) 3610.
[13] C. Adachi, T. Tsutsui, S. Saito, Optoelectronics 6 (1991) 25.
[14] J. Littman, P. Martic, J. Appl. Phys. 72 (1992) 1957.
[15] T. Mori, K. Miyachi, T. Mizutani, J. Phys. D: Appl. Phys. 28 (1995) 1461.
[16] H. Murata, C.D. Merritt, Z.H. Kafafi, IEEE J. Select. Topics Quant. Elect. 4 (1998) 119.
[17] K. Yamashita, J. Futenma, T. Mori, Synth. Met. 111 (2000) 87.
[18] I.G. Hill, A. Kahn, J. Appl. Phys. 85 (1999) 6589.
[19] T. Imai, H. Ishii, Y. Ouchi, Y. Shirota, K. Seki, IEICE Trans. Fundam. E82-A (1999) 1.
[20] C. Adachi, M.A. Baldo, S.R. Forrest, J. Appl. Phys. 87 (2000) 8049.
[21] M.A. Baldo, C. Adachi, S.R. Forrest, Phys. Rev. B 62 (2000) 10967.
[22] G. Gustafsson, Y. Cao, G.M. Treacy, F. Klavetter, N. Colaneri, A.J. Heeger, Nature 357 (1992) 477.
[23] S. Karg, J.C. Scott, J.R. Salem, M. Angelopoulos, Synth. Met. 80 (1996) 111.